

pubs.acs.org/JPCA Article

Electronic Structure and Ligand Effects on the Activation and Cleavage of N₂ on a Molybdenum Center

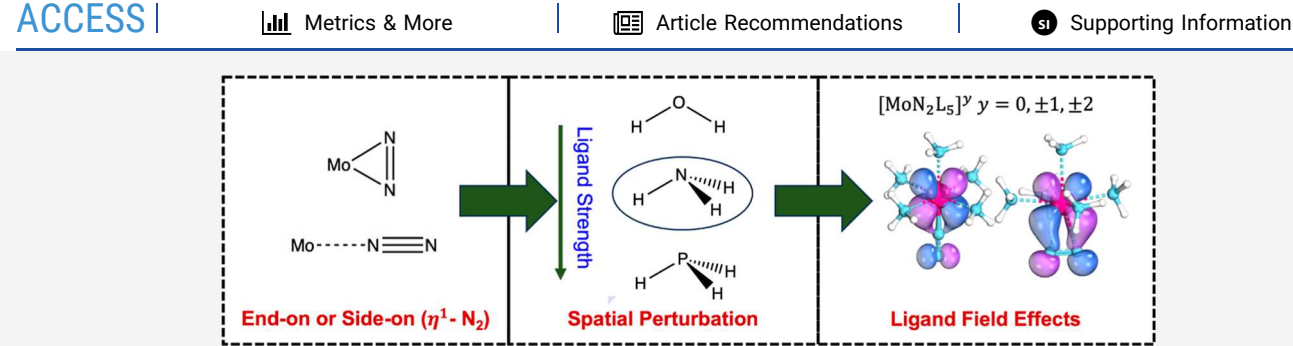
Published as part of The Journal of Physical Chemistry A virtual special issue "Roland Lindh Festschrift".

Maria V. White, Emily E. Claveau, Evangelos Miliordos,* and Konstantinos D. Vogiatzis*



Cite This: J. Phys. Chem. A 2024, 128, 2038–2048





ABSTRACT: Dinitrogen fixation under ambient conditions remains a challenge in the field of catalytic chemistry due to the inertness of N_2 . Nitrogenases and heterogeneous solid catalysts have displayed remarkable performance in the catalytic conversion of dinitrogen to ammonia. By introduction of molybdenum centers in molecular complexes, one of the most azophilic metals of the transitional metal series, moderate ammonia yields have been attained. Here, we present a combined multiconfigurational/density functional theory study that addresses how ligand fields of different strengths affect the binding and activation of dinitrogen on molybdenum atoms. First, we explored with MRCI computations the diatomic Mo-N and triatomic $Mo-N_2$ molecular systems. Then, we performed a systematic examination on the stabilization effects introduced by external NH_3 ligands, before we explore model neutral and charged complexes with different types of ligands (H_2O , NH_3 , and PH_3) and their consequences on the N_2 binding and activation.

1. INTRODUCTION

The catalytic transformation of ammonia from atmospheric dinitrogen in biological nitrogen fixation has inspired many studies on N₂ functionalization. N₂ functionalization poses a variety of challenging problems given the strong N≡N triple bond, chemical inertness, and a significant HUMO−LUMO energy gap (10.82 eV). Active sites bearing transition metals have displayed high reactivity toward N₂ valorization through the (electro)catalytic conversion to ammonia. Artificial nitrogen fixation systems utilizing molecular catalysts bearing vanadium, iron, molybdenum, truthenium, and other metals have been the subject of extensive experimental effort and have facilitated the catalytic generation of NH₃ under mild environment conditions as opposed to the Haber–Bosch industrial process.

Over the past 50 years, many dinitrogen metal complexes, including both mononuclear and binuclear metal active sites, have been synthesized. 9,10 In 2003, Yandulov and Schrock achieved homogeneous catalytic ammonia production using a well-defined tri(amido)amine Mo(III) complex. Nishibayashi et al. examined the application of molybdenum complexes containing N-heterocyclic carbene-based PCP-type pincer ligands. Within this group of complexes, the molybdenum

trichloride complex with a trifluoromethyl group emerged as the most effective catalyst for ammonia production. Remarkably, this catalyst exhibited the capability to produce up to 60,000 equivalents of ammonia. In 2011, Nishibayashi reported a low-valent Mo—phosphine catalyst for ammonia synthesis. One promising approach to ammonia production utilizes molybdenum as a catalyst in conjunction with samarium diiodide and either alcohols or water. The molybdenum catalyst enables the production of a significant quantity of ammonia, with the potential to generate up to 4350 equiv.

Depending on the type of the molecular complex and the conditions of the reaction, N_2 can bind to one or two transition metals through different modes. ^{9,10} In the case of one metal center, end-on or side-on (η^1-N_2) binding of N_2 can activate the triple bond, elongate it, and render it prone to

Received: November 28, 2023 Revised: January 31, 2024 Accepted: February 2, 2024 Published: March 6, 2024





functionalization via the formation of N–H bonds. A typical example is the end-on mechanism adopted by nitrogenases.
The mononuclear terminal end-on binding mode is more common. Typically, the activation entails a σ - and π -donation from the dinitrogen moiety to the metal and back-bonding from the metal d orbitals to σ^* - and π^* -orbitals. The back-donation to σ^* is thought to be more significant.
The back-donation to σ^* is thought to be more significant.
In the case of two metal centers, an activated bridging dinitrogen complex is formed.
The some cases, the complete cleavage of the N_2 has been achieved by the concerted action of two metal centers.
The replacement of the two formed metal-nitrogen bonds with six N–H bonds follows. Another perspective is the activation of N_2 (and other small molecules) via low-coordinate metal complexes.

Despite the extended experimental work in the literature, the role of the metallic charge (or oxidation state) and that of the ligands needs to be understood better for further improvement of the catalysts. Here, we focus on single molybdenum centers to provide some initial systematic theoretical investigation. Different models have recently been developed to elucidate the activity of terminal monometallic N_2 complexes as opposed to bridging bimetallic N_2 complexes. To these ends, we extend our previous theoretical study of the Mo atoms and ions $(0, \pm 1, \pm 2) + N_2$ reaction in two different directions. First, we explore the negatively charged single metal centers, which have recently been found to have superior performance for other significant chemical processes, such us methane to methanol transformation. 31,32 Second, we add ligands in a systematic manner and, finally, study the effects of various ligands for saturated complexes. Although many effective ligands, such as PNP-type pincer ligands and cyclic alkyl amino carbene-based ligands, have been developed to facilitate N2 activation, the direct effects of peripheral ligands of the metal site remain relatively unexplored, which are crucial in determining the extent of N-N activation. Significant variations in reactivity can result from even minor variations in the ligand's electronic structure and steric geometry. Our previous and present multiconfigurational studies demonstrate that a reduced (electron rich) Mo center of the side-on MoN₂ complex leads to a greater degree of N₂ activation, ³³ and it can actually cleave the N≡N bond.

A fundamental understanding of the ligand—metal environment that can bind and activate dinitrogen with the precise affinity while also displaying the necessary selectivity, reactivity, and stability is a difficult task in chemistry. This reason, we present a comprehensive study that connects bare metal Mo–N₂ molecular species to ligated complexes with terminal end-on (η^1 -N₂) and side-on (η^2 -N₂) binding modes. A detailed molecular orbital analysis was performed for the elucidation of ligand field effects on the ground and redox states of pseudo-octahedral [MoN₂L₅]^x molecular model complexes ($x = 0, \pm 1, \pm 2$) where L corresponds to ligands of variable strength that are considered in this study.

2. METHODS

The state-specific and state-average complete active space self-consistent field $(CASSCF)^{35,36}$ method was applied in the study of the diaotmic MoN. Dynamic correlation was introduced subsequently by means of multireference configuration interaction $(MRCI)^{37,38}$ or second-order perturbation theory (CASPT2). The selected active state is given as CAS(n, m), where n is the number of electrons and m the number of active orbitals. The active space for the diatomic

MoN species includes nine electrons in nine orbitals or CAS(9,9). Specifically, at a long Mo-N distance, these 9 orbitals are the 4d and 5s atomic orbitals of Mo and the 2p atomic orbitals of N. The 2s orbitals of N remain doubly occupied at the CASSCF level. All valence electrons (11 electrons, including the 2s of N) are correlated with the MRCI and CASPT2 levels of theory. Exploratory calculations and potential energy curves (PECs) were completed for states with doublet, quartet, and sextet spin multiplicity using triple- ζ (TZ) basis sets (aug-cc-pVTZ^{39,40} for N and cc-pVTZ-PP⁴¹ for Mo). The latter is combined with a Stuttgart relativistic effective core pseudopotential. The $C_{2\nu}$ point group symmetry elements are exploited for all calculations. Spectroscopic constants were calculated by solving the rovibrational Schrödinger equation with our in-house code (Rovib) using refined PECs at the quintuple- ζ (5Z = aug-cc-pV5Z for N and cc-pV5Z-PP for Mo) basis set. All calculations were carried out with MOLPRO2015 and MOLPRO2021.⁴² A detailed analysis of the electronic states of MoN computed by MRCI is included in the Supporting Information Section S1.3

The analysis of the triatomic MoN_2 began with geometry optimization (MN15/def2-TZVP) across three different spin states (singlet, triplet, and quintet). Optimizations returned all real frequencies. The lowest energy equilibrium geometry (triplet) is used in the multireference calculations to find the equilibrium wave function and to construct the reported PECs. For the multireference calculations, the active space is composed by 12 orbitals, the 2p orbitals of each nitrogen, the 4d and 5s orbitals of molybdenum, which results to a CAS(12,12). The MRCI calculations were performed with C_s symmetry with the cc-pVDZ-pp basis set for Mo and cc-pVDZ on the N atom. Density functional theory (DFT) and MRCI calculations were carried with Gaussian⁴³ and MOLPRO, respectively.

Regarding the $[MoN_2L_5]^x$ molecular model complexes (x = $0, \pm 1, \pm 2$), we performed a DFT screening of the ligand field effects⁴⁴ on the ground and redox states of the side- and endon modes of MoN2. All DFT calculations were performed with the ORCA quantum chemistry software package version 5.0.0. 45.45 For examination of the ligand field effects on the Mo center, we considered three different molecular ligands. The first is H₂O, which is representative of a weak ligand field, NH₃ (moderate strength), and PH₃ (relatively stronger ligand field). Unrestricted geometry optimizations were performed using the def2-TZVPP basis set, 46 the def2-ECP core potential for molybdenum, the auxiliary basis def2/J, ⁴⁷ and the B3LYP density functional, ^{48,49} together with the atom-pairwise dispersion correction based on tight binding partial charges (D4) was used. 50,51 A DefGrid2 and conductor solver model (CPCM) using acetonitrile solvent was applied⁵² in order to simulate experimental conditions. To ensure true energy minima, frequency calculations were performed.

3. RESULTS

3.1. MoN_2 and $(NH_3)_nMoN_2$ (n=1,2,3). Here, we discuss the activation of N_2 with either a single metal atom or low-coordinate ammonia molybdenum complexes. Molybdenum-amine complexes were used for the activation of N_2 . In addition to the linear NMoN and $Mo-N_2$ side-on or end-on geometries examined in our previous work, here we report the bent NMoN structure, where the N-N bond is cleaved focusing on the electronic structure transformations. We initially optimized the geometry for three spin multiplicities

with DFT. The singlet and triplet states adopt a symmetric structure with Mo–N bond lengths of 1.651 and 1.678 Å respectively. Their corresponding N–Mo–N angles are 104.4 and 97.1°. The triplet state is predicted as the ground state, with the singlet being just 0.044 eV higher. The optimized structure of the quintet state has two different bond lengths (1.618 and 1.954 Å) and an angle of 113.2°, and is energetically separated by 2.3 eV.

Using these equilibrium geometries, we then performed MRCI calculations to monitor the electronic structure of the low-lying electronic states and how these are connected to the electronic states of MoN. To this end, we constructed the potential energy profiles along the NMo–N dissociation channel. The initial wave functions were obtained for a geometry with Mo–N bond lengths of 1.67 and 1.69 Å and an angle of 100° to impose the C_s symmetry constraints followed along the chosen dissociation process. The active orbitals of

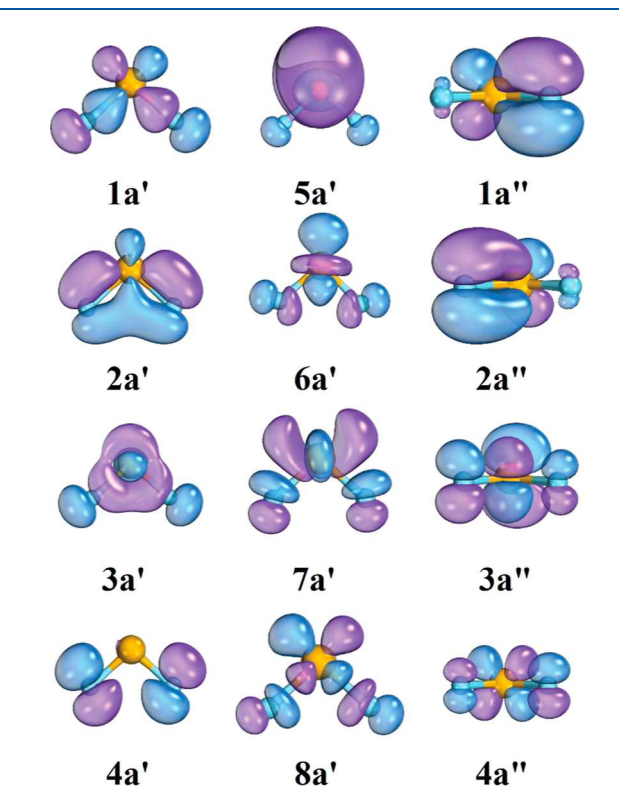


Figure 1. Active molecular orbitals of MoN₂.

the reference CASSCF calculation are listed in Figure 1. The $^1A',\ ^3A',\$ and $\ ^5A'$ states originating from the ground state fragments $MoN(^4\Sigma^-)$ + $N(^4S)$ plus one more $^1A'$ are state-averaged in this calculation. The inclusion of the latter state is important, as demonstrated below, while the remaining $^7A'$

state coming from the same channel was excluded as it is of dissociative nature (no chemical bond between MoN and N).

The 1a' and 3a' orbitals correspond to the σ Mo–N bonds, while 7a' and 8a' are the relative antibonding orbitals. The 1a", 2a", 3a", and 4a" orbitals are the off-plane Mo–N π bonding and antibonding orbitals, whereas 2a', 4a', and 6a' pertain to the three combinations of the one in-plane $2p_{\pi}$ orbital from each nitrogen terminus and one 4d $(4d_z^2)$ of molybdenum. The 5a' is the highly localized 5s of Mo polarized away from the two Mo–N bonds.

The dominant configurations are given in Table 1. At the CASSCF and MRCI levels, the ground state \tilde{X}^1A' is an openshell singlet followed closely by its sibling triplet state (see Figures 2 and 5). In these two states, we can assign two

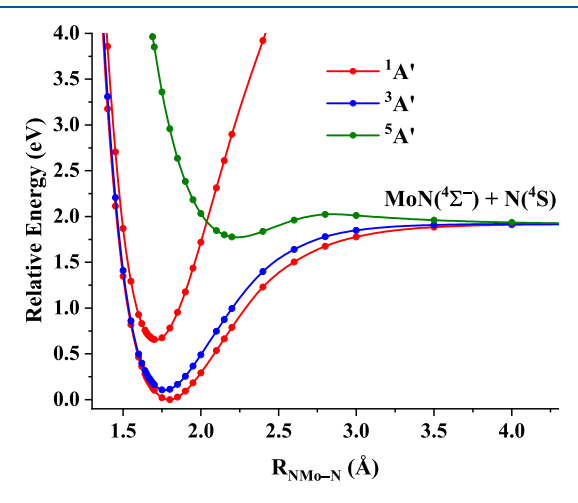


Figure 2. CASSCF potential energy curves of MoN2 as a function of the NMo–N distance $R_{\rm NMo-N}$.

 $\sigma(\text{MoN})$ bonds (1a′² 3a′²), two off-plane $\pi(\text{MoN})$ bonds (1a″² 2a″²), and one in-plane $\pi(\text{MoN})$ bond (2a′²). The two unpaired electrons occupy the polarized 5s(Mo) (5a′¹) and the in-plane 4a′ orbital, which pertain to localized 2p(N) orbitals perpendicular to the Mo–N bonds.

The excited singlet state $^1A'$ is a closed-shell singlet, where the polarized 5s(Mo) electron migrates to the 4a' orbital. Our DFT calculations converged to this singlet state, and therefore, they predicted a triplet ground state. In both DFT and MRCI calculations, the quintet state comes from the triplet state by promoting an electron from 2a'' to 3a'' [$\pi(MoN) \rightarrow \pi^*(MoN)$].

The formation of MoN₂ from MoN + N provides a clearer picture of its chemical bonding. The relative PECs are listed in Figure 2. The ground state of MoN ($^4\Sigma^-$) has a triple bond (σ^2_{MoN} π^4_{MoN} ; see Supporting Information for more details on the electronic structure) and three unpaired electrons localized on the Mo in two $\delta_{\text{Mo}} \sim 4 d_{\text{Mo}}$ and $\sigma_{\text{Mo}} \sim 5 s_{\text{Mo}}$ (see Supporting

Table 1. Dominant Electronic Configurations for the Low-Lying States of MoN₂ (See Figure 1 for Orbitals)

state	coeff.	1a'	2a'	3a'	4a′	5a'	6a'	7a'	8a'	1a"	2a"	3a"	4a"
\tilde{X}^1A'	0.61	2	2	2	α	β	0	0	0	2	2	0	0
	-0.61	2	2	2	β	α	0	0	0	2	2	0	0
$^{3}A'$	0.88	2	2	2	α	α	0	0	0	2	2	0	0
$^{1}A'$	0.84	2	2	2	2	0	0	0	0	2	2	0	0
⁵ A'	0.85	2	2	2	α	α	0	0	0	2	α	α	0

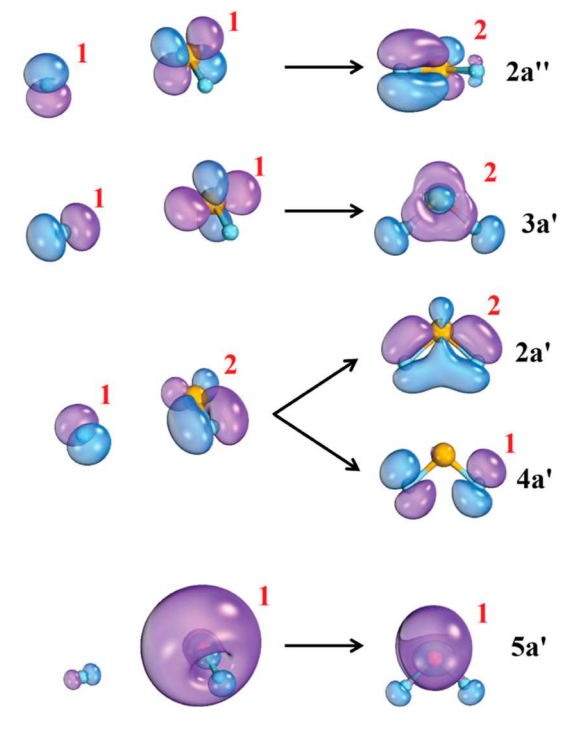


Figure 3. Selected combinations between the 2p orbitals of a N atom approaching MoN and the MoN molecular orbitals. The red colored numbers indicate the number of electrons populating each orbital (more details are provided in the Supporting Information, Section S1).

Information, Section S1). The σ_{MoN} and π_{MoN} orbitals are polarized toward the N terminus signaling an ionic Mo³⁺N³⁻ character. The second incoming N atom has three unpaired electrons $(2p_N^3)$, which can in principle form a triple bond with Mo. Symmetry constraints allow the formation of only two bonds with the two remaining electrons, $2p_N^1$ and $5s_{Mo}^1$, giving rise to the lowest energy open-shell singlet and triplet states. The specific orbital combinations are depicted in Figure 3. The two formed bonds correspond to the 2a" and 3a' bonds (specifically, the two σ_{MoN} bonds are combined to give 1a' and 3a'; see Figure 1). The two unpaired electrons are well localized on Mo (5a') and N atoms (4a'). Overall, the chemical bonding in the first two states can be succinctly assigned as $N \equiv Mo^{\bullet} = N^{\bullet} \leftrightarrow N^{\bullet} = Mo \equiv N$ or by considering the ionic character of the system N^{3} - $Mo^{\bullet 5}$ + $N^{\bullet 2}$ - \leftrightarrow $N^{\bullet 2-}Mo^{\bullet 5+}N^{3-}$.

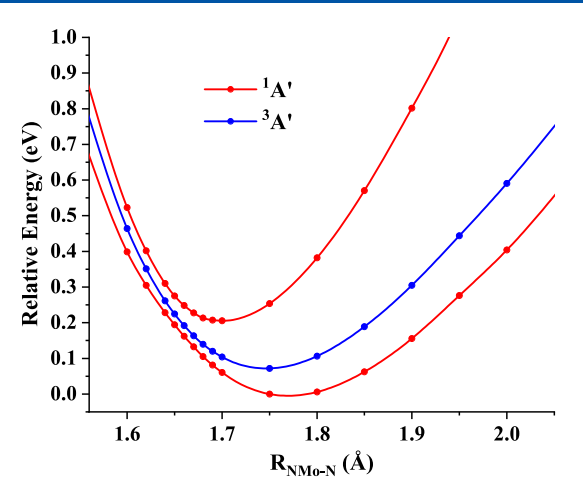


Figure 5. MRCI potential energy curves of MoN₂ around equilibrium as a function of the NMo-N distance $R_{\text{NMo-N}}$.

As stated earlier, the excited $^1A'$ state is a closed shell state and can be produced from the ground state \tilde{X}^1A' by promoting the Mo unpaired electron to the nitrogen termini $(5a' \rightarrow 4a')$. Therefore, the bonding in this state is more ionic and can be seen as N^3 – Mo^6 + N^3 –. The PEC of this state is steeper and, at long distances, goes to $MoN^+ + N^-$. Finally, the excitation energy of this state drops significantly when dynamic electron correlation is included. The MRCI PECs of Figure 5 are indicative, where the singlet excited state is only 0.2 eV higher than the ground singlet state (was 0.67 eV at CASSCF; see Figure 2), and the two PECs actually form an avoided crossing at 1.65 Å. The energy difference between the triplet state and this closed-shell singlet at MRCI is 0.13 eV (which was 0.58 eV at CASSCF).

We turn now our attention to the different conformations of the MoN_2 triatomic molecule and their relative energies for both the neutral and the anionic species. The left side of Figure 4 shows the relative energies for three different species of [Mo,2N] composition, the $Mo+N_2$ fragments, the end-on and side-on $Mo(N_2)$ isomers, and the bent NMoN molecule. The energies of the end-on species are shown with dashed horizontal lines, and they are higher in energy than the side-on. The NMoN species, where N_2 is cleaved, is higher in energy than both $Mo(N_2)$ and $Mo+N_2$ for all spin states. The addition of an electron to the system changes the energetics thoroughly, and now, the bent NMoN $^-$ species is lower in energy than any other structure. This result indicates that

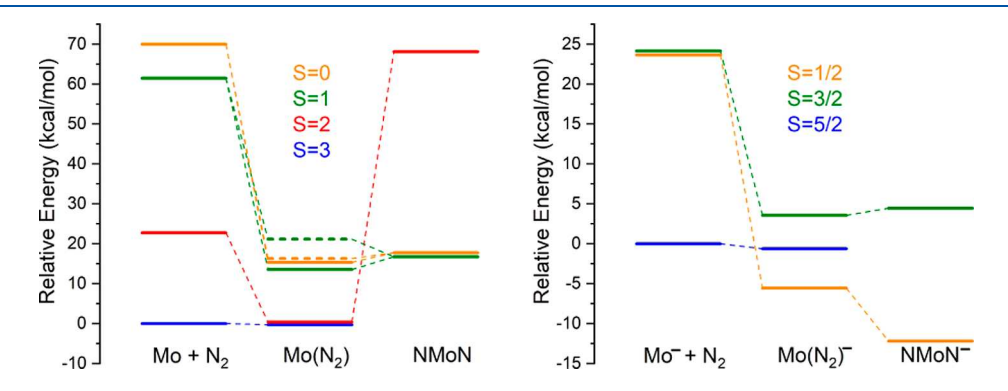


Figure 4. Relative energies of the side-on and end-on (dashed lines) $Mo(N_2)^{0,-}$ and bent $NMoN^{0,-}$ species with respect to $Mo^{0,-} + N_2$ for various spin states, as computed with the MN15 density functional.

electron rich metal centers facilitate the activation of dinitrogen and can lead to a new class of reactive molecular structures (electron rich monometallic low-coordinate complexes) for the activation of N_2 . This also indicates that single metal atom catalysts (metals supported on a surface) will demonstrate higher performance in electrocatalytic processes. 53,54

The higher formal charge of Mo in the closed-shell singlet state [Mo(VI) vs Mo(V) for the other two states] suggests that coordination with NH3 ligands will stabilize this spin state over the intermediate or high spin states. To corroborate this thought, we optimized the geometries of the $(NH_3)_nMoN_2$ complexes with n=1,2, and 3. We considered the closed-shell singlet and the triplet states at the MN15 level of theory with the cc-pVDZ-PP basis set on Mo and aug-cc-pVDZ basis on N and H. Our attempts to add a fourth ammonia ligand in the first coordination sphere of Mo resulted in a $MoN_2(NH_3)_3 + NH_3$ structure, where the fourth ammonia resides in the second coordination sphere. All structures and frequencies are reported in the Supporting Information, Section S3. The closed-shell singlet—triplet energy gap ΔE as a function of n is plotted in Figure 6. Positive/negative ΔE

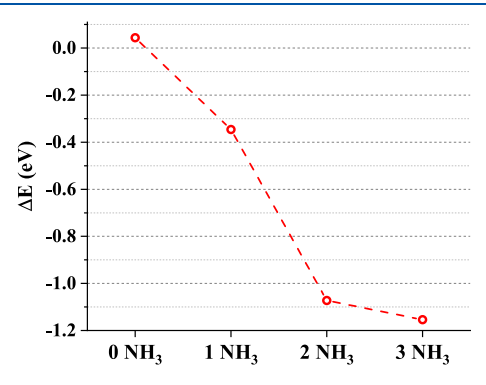


Figure 6. Energy difference ΔE between the closed-shell singlet and the triplet states of MoN₂ ligated with no, one, two, and three ammonia molecules at MN15.

indicates that the closed-shell singlet is higher/lower in energy. Indeed, the addition of ammonia ligands stabilizes the singlet state considerably. ΔE is 0.044 eV for n=0 and turns negative with just one ammonia ligand (-0.34 eV). ΔE increases (in absolute value) to -1.07 eV for n=2 and changes only slightly to -1.15 eV for n=3. In conclusion, ammonia stabilizes the complex with both terminal metal nitridos, which has a larger oxidation state on the metal. Below, we consider the effect of more ligands and the oxidation state of Mo by changing the overall charge of the complex in the N_2 activation process.

3.2. Ligand Field Effects. The study presented herein investigates the influence of the ligand field on a pseudo-octahedral molybdenum coordination complex, with specific focus on the presence of a dinitrogen ligand in either an axial terminal end-on or side-on configuration. For each complex, a range of distinct spin states were taken into consideration along with a variety of ligands of various strengths such as H₂O, NH₃, and PH₃, ranging from weak (H₂O) to moderate (NH₃) and ultimately to strong ligands (PH₃). The selection of a ligand environment plays a crucial role in determining the properties and reactivity of metal complexes and the relative binding strength or affinity of a ligand toward a central metal ion. The influence of the ligand field effects on the metal center

is discussed, offering valuable insights of the electronic structure, bonding properties, and reactivity of these molecular systems, and even the possibility for chemical transformations. An explicit solvation model was applied in our calculations using acetonitrile, a medium-polar solvent commonly used in heterogeneous catalysis. ^{13,55} A short discussion on the solvent effect is given in Supporting Information, Section S4.

The following analysis only encompasses systems that maintain a six-coordinate environment upon optimization with B3LYP-D4/def2-TZVPP. Our discussion begins by examining the molecular systems with a weak field ligand (H2O) and dinitrogen, and we differentiate the various complexes by considering how dinitrogen binds to the molybdenum center. The molecular orbitals of the reduced states of $[MoN_2(H_2O)_5]^n$ (n = 1+, 2+) are shown in Figure 7 (end-on mode) and Figure 8 (side-on mode), which qualitatively display the distribution of electrons and the splitting of the d orbitals. The doublet (1+) complex bearing the end-on mode of dinitrogen exhibits an electronic configuration of $(\sigma)^4(\pi)^4(d_{xy})^1(\pi^*)^0(\sigma^*)^0$. The side-on mode of dinitrogen introduces symmetry restrictions, which are visually represented by the electronic configuration $(\sigma)^4(\pi)^2(d_{yy})^2(d_{yz})^1(\pi)^0(\sigma)^0$.

The most stable end-on $[MoN_2(H_2O)_5]^{2+}$ complex with a 2+ charge has a triplet ground spin state with a $(\sigma)^4(\pi)^3(\mathrm{d}_{xy})^1(\pi^*)^0(\sigma^*)^0$ configuration. The extra electron that is lost from the 1+ complex can be removed either from the nonbonding dxy orbital, leading to a singlet ground spin state, or from one of the bonding π orbitals, which leads to a triplet ground spin state. We found that these two states are close in energy (0.13 eV; see Supporting Information, Section S5), favoring the triplet spin state. The 4d orbitals of molybdenum are close in energy in the presence of a weak ligand field generated by the five H₂O ligands, and thus, the triplet spin state is more stable due to exchange interactions between the two unpaired electrons. The triplet (2+) ground state bearing the side-on mode of N2 displays a $(\sigma)^4(\pi)^2(d_{xy})^1(d_{yz})^1(\pi)^0(\sigma)^0$ electronic configuration. A higher degree of activation is observed in the N2 side-on complexes. Specifically, the bond distances for the side-on Mo(I) and Mo(II) complexes are 1.220 and 1.155 Å, respectively. These values contrast with the bond distances of 1.160 and 1.117 Å observed in the end-on dinitrogen complexes. Steric effects may be more pronounced when bulkier equatorial ligands are present. Therefore, the terminal end-on mode of N₂ opens up broader avenues of reactivity, as it has been demonstrated in a variety of molecular Mo catalysts.²⁰ This mode enables the existence of additional catalytic binding pathways, such as facilitating protonation of the terminal nitrogen atom, particularly after N₂ activation.

In relation to cationic states, the Mo(II) species demonstrates its greatest stability when it adopts the end-on N_2 configuration. This is consistent for all systems presented in Tables 2 and 3. For example, for the $[MoN_2(H_2O)_5]^{2+}$ case, the coordination of N_2 to pseudo square pyramidal bare complex is $\Delta E_{\rm coord} = -0.89$ eV, while the corresponding value for the side-on conformer is -0.62 eV. The calculations of binding energy were conducted using the stable pseudo square pyramidal bare complex as the reference geometry. However, among the species with a 1+ charge, none of the stable spin

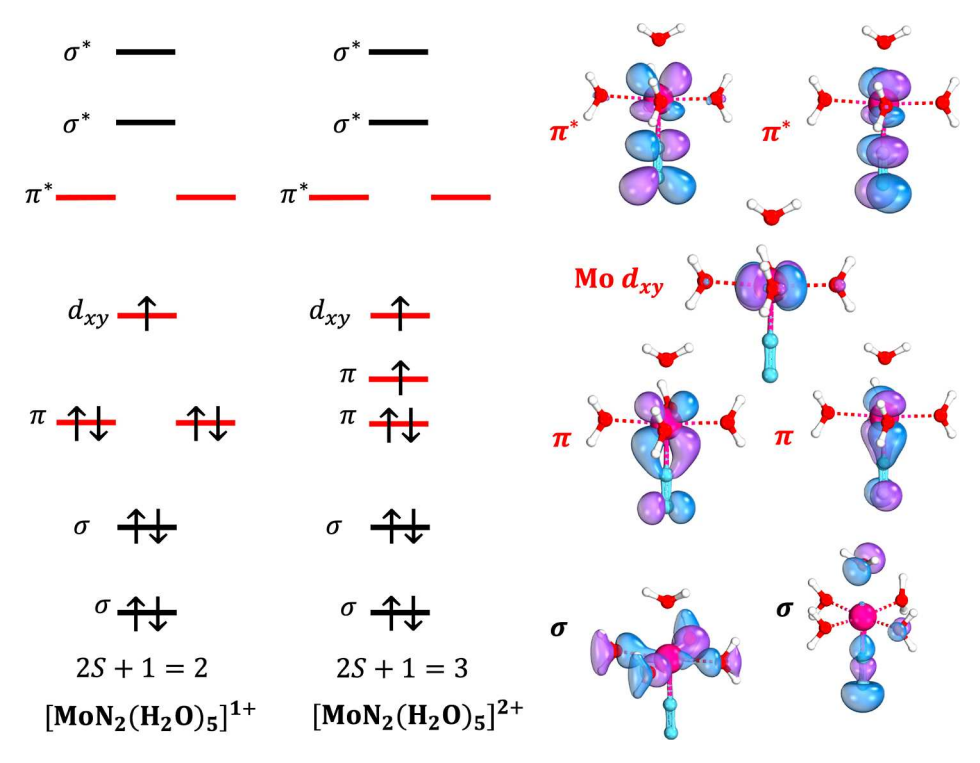


Figure 7. Molecular orbital diagrams (B3LYP-D4/def2-TZVPP) corresponding to pseudo-octahedral molecular complexes of the end-on $[MoN_2(H_2O)_5]^x$ where x = +1, +2 denotes the charge. Orbitals with different occupation numbers across the molecular series examined in this work are shown in red color.

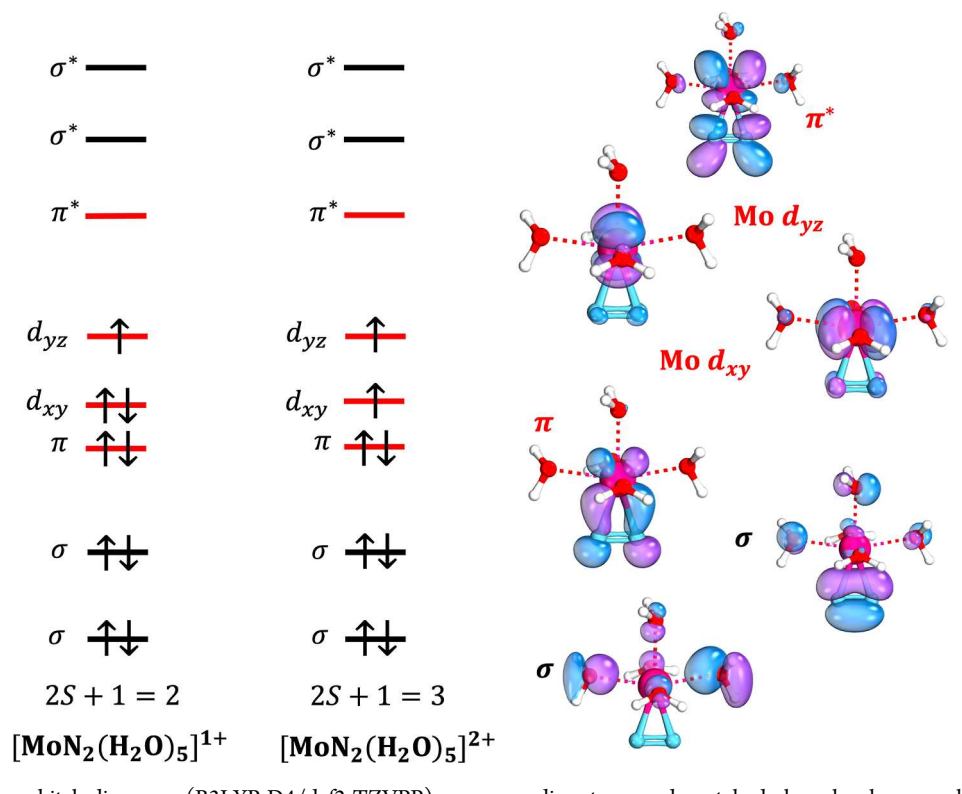


Figure 8. Molecular orbital diagrams (B3LYP-D4/def2-TZVPP) corresponding to pseudo-octahedral molecular complexes of the side-on $[MoN_2(NH_3)_5]^x$, where x = +1, +2 denotes the charge. Orbitals with different occupation numbers across the molecular series examined in this work are shown in red color.

states exhibited this particular geometry since the square pyramidal geometry was distorted. As a result, the binding energy for such cases could not be determined computationally. This observation suggests that Mo tends to favor a complete coordination sphere in the presence of water molecules. 10 Additionally, the presence of axial dinitrogen

Table 2. N_2 Coordination Energies ($\Delta E_{\rm coord}$), IPs, EAs (in eV), and Key Interatomic Distances (in Å) of the Bound Ligated Pseudo-Octahedral Molecular Complexes with the N_2 End-On Mode Computed with B3LYP-D4/def2-TZVPP

complex	R_{N-N}	$R_{\mathrm{Mo-N}}$	2S + 1	$\Delta E_{\mathrm{coord}}$	IP^a	EA ^b
$[MoN_2(H_2O)_5]^{1+}$	1.160	1.868	2	_ <i>c</i>		
$[MoN_2(H_2O)_5]^{2+}$	1.117	1.981	3	-0.89	7.47	
$[MoN_2(NH_3)_5]^0$	1.210	1.826	1	-2.20		
$[MoN_2(NH_3)_5]^{1+}$	1.173	1.865	2	-2.70	1.02	
$[MoN_2(NH_3)_5]^{2+}$	1.126	1.956	3	-1.21	3.94	
$[MoN_2(NH_3)_5]^{1-}$	1.181	1.858	2	-2.32		-0.69
$[MoN_2(NH_3)_5]^{2-}$	1.217	1.823	1	-2.56		-1.23
$[\mathrm{MoN}_2(\mathrm{PH}_3)_5]^0$	1.124	2.002	1	-1.47		
$[MoN_2(PH_3)_5]^{1+}$	1.112	2.046	2	-1.16	3.90	
$[MoN_2(PH_3)_5]^{2+}$	1.102	2.102	3	-0.93	8.61	
$[MoN_2(PH_3)_5]^{1-}$	1.173	2.222	2	-0.26		-1.00

^aIP values with respect to the neutral complexes, except for the water complex, which are computed with respect to $[MoN_2(H_2O)_5]^{1+}$. ^bEA values with respect to the neutral complexes. ^cNo $\Delta E_{\rm coord}$ was computed since geometry optimization of the bare $[MoN_2(H_2O)_5]^{1+}$ resulted in an uncoordinated H_2O ligand.

Table 3. N_2 Coordination Energies ($\Delta E_{\rm coord}$), Ips, Eas (in eV), and Key Interatomic Distances (in Å) of the Bound Ligated Pseudo-Octahedral Molecular Complexes with the N_2 Side-on Mode Computed with B3LYP-D4/def2-TZVPP

complex	R_{N-N}	$R_{\text{Mo-N}}$	2S + 1	$\Delta E_{\rm coord}$	IP^a	EA ^b
$[MoN_2(H_2O)_5]^{1+}$	1.220	2.004	2	_c		
$[MoN_2(H_2O)_5]^{2+}$	1.155	2.149	3	-0.62	5.40	
[MoN2(NH3)5]0	1.232	2.014	3	-1.65		
$[MoN_2(NH_3)_5]^{1+}$	1.229	2.012	2	-2.37	0.80	
$[MoN_2(NH_3)_5]^{2+}$	1.162	2.157	3	-1.02	3.57	
$[MoN_2(NH_3)_5]^{1-}$	1.235	2.016	2	-1.90		-0.82
$[MoN_2(NH_3)_5]^{2-}$	1.236	2.017	3	-1.92		-1.14
[MoN2(PH3)5]0	1.137	2.312	1	-0.75		
$[MoN_2(PH_3)_5]^{1+}$	1.148	2.217	2	-0.69	3.64	
$[MoN_2(PH_3)_5]^{2+}$	1.125	2.335	3	-0.37	8.46	

^aIP values with respect to the neutral complexes, except for the water complex, which are computed with respect to $[MoN_2(H_2O)_5]^{1+}$. ^bEA values with respect to the neutral complexes. ^cNo $\Delta E_{\rm coord}$ was computed since geometry optimization of the bare $[MoN_2(H_2O)_5]^{1+}$ resulted in an uncoordinated H_2O ligand.

helps stabilize the complex. The greater stability of the Mo(II) complexes with an end-on configuration compared with the Mo(II) side-on complexes is further supported by the observed second ionization potentials (IPs). The IP values listed in Tables 2 and 3 indicate that the Mo complexes with an end-on configuration have a higher IP (7.47 eV) compared to the side-on analogue (5.40 eV). From Figures 7 and 8, we find that for the side-on conformer, the second electron is lost from the nonbonding $4d_{xy}$ orbital. On the contrary, for the end-on case, the electron is removed from a π orbital of N_2 , which destabilizes its electronic structure, and thus, it leads to a significantly higher IP. Similarly, we should also note that the first ionization energies have not been computed due to the instability of the neutral complex.

3.3. Ammonia and Phosphine Ligated Dinitrogen Complexes. Next, we focus on the $[MoN_2(NH_3)_5]^x$ (x = 0, ± 1 , ± 2) dinitrogen complexes. The molecular orbital diagrams of all molecular species with a five-amine ligand sphere, as obtained by DFT computations, are given in Figure 9. These

configurations were further validated by higher-level multiconfigurational CASSCF calculations (Supporting Information, Section S7). The neutral end-on N₂ complex has a singlet ground spin state with a $(\sigma)^4(\pi)^4(d_{xy})^2(\pi^*)^0(\sigma^*)^0$ electronic configuration. Similarly to the water-ligated systems, the degeneracy of the π orbitals is broken in the side-on complex. The π -type orbitals between Mo and N₂ are formed from the 4d_{xz} orbital and the π^2 orbitals of dinitrogen, while the 4d_{yz} has less participation to the bonding with N₂.

Upon electron loss, the NH3-ligated complexes with a positive 1+ charge exhibit a structural trans-effect since an electron is lost from the nonbonding 4d_{xy} orbital.⁵⁶ This effect causes elongation of the axial Mo-NH₃ ligand. For example, in the case of the end-on complex, the Mo distance from the axial ammonia ligand is R_{ax} = 2.349 Å, and the average Mo distance from the equatorial ammonia ligands is $R_{\rm eq} = 2.274$ Å, while the Mo- N_2 ligand is 1.865 Å. This effect is not observed in the 2+ charged complexes where the second electron is lost from the π system and the exchange interaction is maximized by the occupancy of the Mo dxy nonbonding orbital minimizing steric effects. For this complex, the $R_{\rm ax}$ and $R_{\rm eq}$ distances are comparable (2.266 and 2.246 Å, respectively, and the Mo-N₂ distance is 1.976 Å). In the 2+ case, all ammonia ligands have relatively similar bond distances. The $\Delta E_{\rm coord}$ between the pseudo square pyramidal complex and the end-on N_2 mode is -2.70 eV, whereas the $\Delta E_{\rm coord}$ with the side-on N_2 configuration is -2.37 eV (vide infra). The IP of the Mo(I) complex bearing the end-on N2 mode is 1.02 eV, while the Mo(II) species displays a higher IP of 3.94 eV. Likewise, the IPs of the side-on $[MoN_2(NH_3)_5]^{1+}$ and $[MoN_2(NH_3)_5]^{2+}$ complexes are 0.80 and 3.57 eV, respectively (Tables 2 and 3). This trend is consistent with the behavior observed in the water complexes, where the complexes with the end-on mode of dinitrogen exhibit greater stability and reduced susceptibility to oxidation. The anionic states are characterized by the presence of a populated Rydberg orbital, which relates to the solvation of an electron by the ammonia ligands (see Figures S3 and S4 of the Supporting Information, Section S6). Such diffuse peripheral electrons have been observed experimentally for alkali and alkaline earth metal ammonia complexes⁵⁷ and have been predicted for transition metal complexes, 60 including $[Mo(NH_3)_6]^{0,1+}.^{61}$ Complexes featuring the end-on mode of dinitrogen display a doublet electronic configuration as $(\sigma)^4(\pi)^4(d_{xy})^2(Ryd)^1(\pi)^0(\sigma)^0$ in the 1- species. Conversely, in the singlet state 2-, the configuration is $(\sigma)^4(\pi)^4(d_{xy})^2(Ryd)^2(\pi)^0(\sigma)^0$. A weaker ΔE_{coord} is observed with N₂ in the anionic cases. Both 2- dinitrogen complexes demonstrate increased electron affinities (EA). Importantly, the end-on complex displays a more negative EA, indicating a preference for the end-on mode. Among these complexes, the Mo(I) end-on complex achieves the highest stability, characterized by an activated N₂ bond length of 1.1727 Å.

Before we end our discussion on the complexes with ammonia ligands, we provide a short note on the two molecular systems with the strongest $\Delta E_{\rm coord}$. For both end-on and side-on conformations, the monocationic complexes have the most negative interaction energies with N₂ (-2.70 and -2.37 eV, respectively). In addition, both systems have a relative low IP (about 1 eV) and, in contrast to the anionic cases, both exhibit a stable electronic structure with bound electrons. The difference between the two $\Delta E_{\rm coord}$ values shows

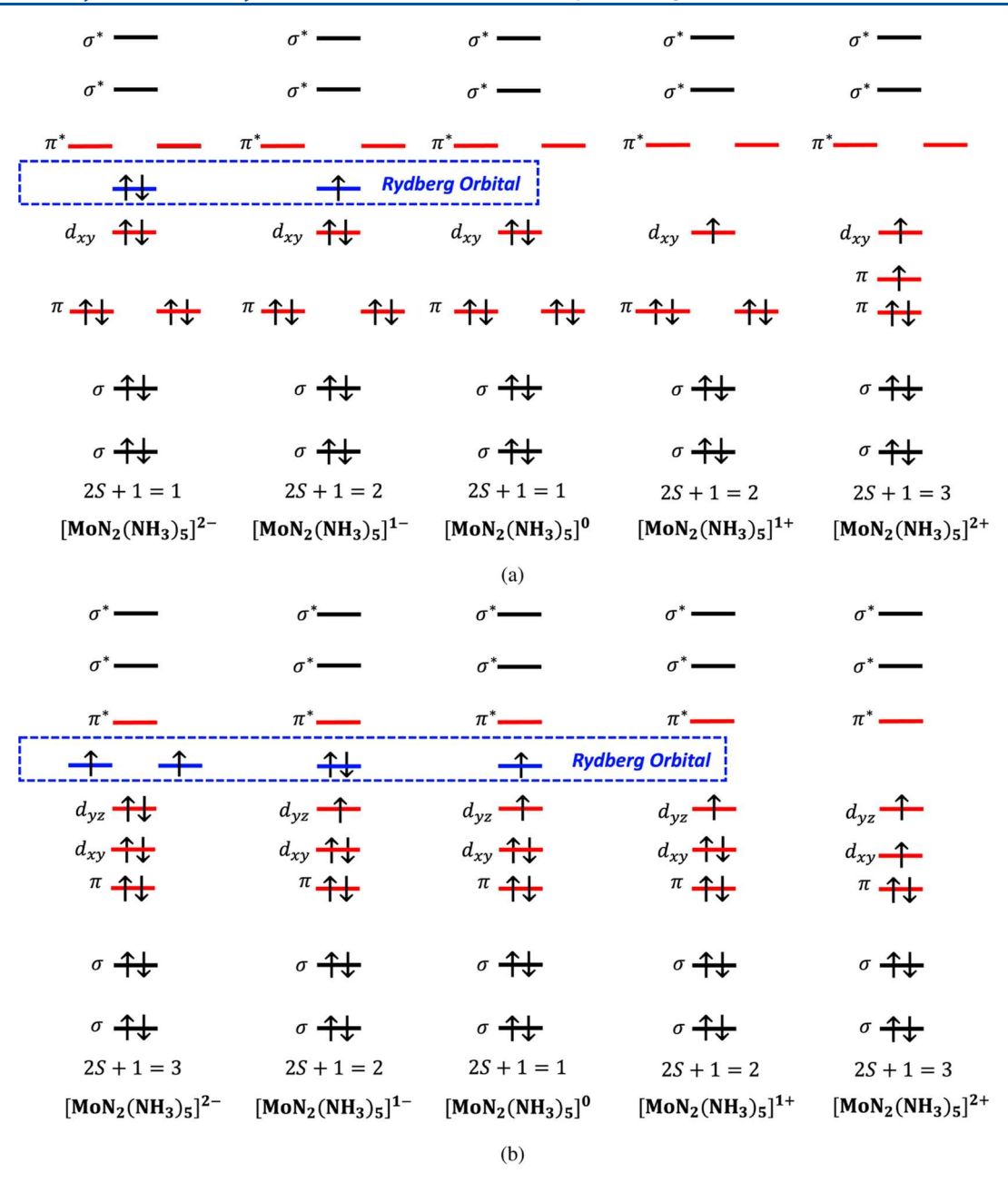


Figure 9. Molecular orbital diagrams of $[MoN_2(NH_3)_5]^x$ ($x = 0, \pm 1, \pm 2$) pseudo-octahedral molecular complexes with N_2 in the (a) end-on and (b) side-on mode.

a more preferable end-on configuration, which can be explained from their electron occupation and the energies of the molecular orbitals. The DFT-computed energies of the key highest-occupied molecular orbitals are shown in Figure S6 of the Supporting Information. For the end-on case, the doubly degenerate π_x and π_y orbitals formed between the $4d_{xz/yz}$ atomic orbitals of Mo and the π^* of the dinitrogen molecule are doubly occupied, and they are characteristic of π backbonding between the transition metal and the N2 molecule. For this molecular system, a beta electron hole is found on the nonbonding $4d_{xy}$ atomic orbital of the molybdenum atom. The degeneracy between the two π orbitals is lifted in the side-on case, where the π_x has a lower energy, while the π_v is less stable, and has a predominant $4d_{vz}$ character, and it is singly occupied. Thus, the presence of three electrons on the bonding molecular orbitals leads to a lower

 $\Delta E_{\rm coord}$ for dinitrogen in the side-on case. When we move to the neutral side-on species, the additional electron is not bound to the molecular complex since it occupies a Rydberg orbital, which leads to an even lower interaction energy ($\Delta E_{\rm coord} = -1.65$ eV). On the contrary, the N $_2$ coordination becomes more favorable for the two anionic complexes since an additional electron occupies the 4d $_{\rm yz}$ orbital that has a small but non-negligible π -bonding character ($\Delta E_{\rm coord} = -1.90$ and -1.92 eV, respectively). Similar arguments hold for the end-on cases, where all $\Delta E_{\rm coord}$ range between -2.20 and -2.70 eV except the [MoN $_2$ (NH $_3$) $_3$] $^2+$ complex that has lost an electron from the π bonding orbital ($\Delta E_{\rm coord} = 1.21$ eV).

Last, we discuss the results for the pseudo-octahedral complexes of MoN₂ with phosphines, the stronger of the three ligands considered in this study. Both the end-on and side-on modes of dinitrogen in these complexes exhibit qualitative

molecular orbital diagrams comparable to those in the two other cases. The neutral species exhibits the strongest $\Delta E_{\rm coord}$ (-1.47 eV) with the end-on mode of N_2 unlike the cases bearing the weak and moderate ligand. The 1+ doublet and 2+ triplet share the same electronic structure description and dorbital splitting properties as the water- and ammonia ligated cases. The IP values for the 1+ and 2+ states were found at 3.90 and 8.61 eV, respectively, exhibiting a consistent behavior for all complexes with the end-on mode of N2. Similarly, the complexes with the side-on mode of N2 showed IPs of 3.64 and 8.46 eV, respectively. In the anionic 1- doublet ground state, N2 is not bound on the Mo center, as reflected by the weak $E_{\rm int}$ of -0.26 eV. The optimized geometry revealed a N-Mo-N angle of 138.573° that is significantly different from the side-on conformation. The electronic configuration of this complex is $(\sigma)^4(\pi)^4(d_{xy})^2(\pi^*)^1(\sigma)^0(\sigma^*)^0$ (see Supporting Information, Section S9 for qualitative molecular orbital diagrams), and the added electron was found on the N₂ antibonding orbital, and not on a Rydberg orbital as in the case of the anionic complexes with NH₃ ligands. This is due to the ability of ammonia ligands to solvate electrons as opposed to phosphine which facilitate π -back bonding instead. The $[MoN_2(PH_3)_5]^{1-}$ complex exhibits low degree of N_2 activation, with a bond length of 1.173 Å, which is probably not due to the Mo center but due to the extra electron on the antibonding π^* orbital. Further reduction released N_2 from the model complex, and thus, the 2- case has not been further analyzed. The discussion does not include the anionic species of the sideon N2 complexes since DFT geometry optimizations resulted to structures with an unbound N₂ molecule.

Finally, a comparison of the computed $\Delta E_{\rm coord}$ values between the three different ligand types considered in this study (H₂O, NH₃, and PH₃) for the dicationic complexes leads to an interesting observation. For the weakest ligand (H₂O), a $\Delta E_{\rm coord} = -0.89$ eV was obtained from B3LYP-D4/def2-TZVPP, the stronger ammonia ligand lead to a $\Delta E_{\rm coord}$ of -1.21 eV, while the strongest phosphines lead to a decreased $\Delta E_{\rm coord}$ value of -0.96 eV. Both water and ammonia ligands coordinate to the Mo center through forward donation. On the contrary, the stronger phosphine ligands have a significant amount of π -backdonation since the LUMO of PH₃ can accept electrons from the 4d orbitals of Mo, which is reflected on the lower interaction energy of the complex with N₂, when it is compared to the NH₃ case.

4. DISCUSSION AND CONCLUSIONS

In this paper, we have examined the Mo-N bond in the ground and excited electronic MoN and NMoN species (the N-N bond is cleaved). We showed that the complete dissociation of the N2 bond is possible for anionic unsaturated/low-coordinate molybdenum monometallic molecular complexes and that ammonia ligands stabilize the $N^{3-}Mo^{6+}N^{3-}$ over $N^{3-}Mo^{\bullet 5+}N^{\bullet 2-}$. This is the first time that a single metal atom is found to cleave the triple N2 bond bypassing the concerted action of two molybdenum centers reported in the literature²⁵ or larger metallic clusters (see for example ref 63). Then, we explored saturated hexacoordinated complexes and the relative stability of side-on and end-on isomers with three different ligand types (H₂O, NH₃, and PH₃) and different charges (neutral, anionic, and cationic). All complexes that yielded a N₂ molecule bound on the Mo center were further analyzed and discussed. In particular, we focused

on the electronic structure, the $\Delta E_{\rm coord}$ between the Mo model complex and N₂, as well as the level of the N₂ activation. From our analysis, we found that the end-on cationic complex with NH₃ ligands has the strongest $E_{\rm int}$ across the molecules considered here (-2.70 eV). An interesting observation is that the extra electrons on the anionic species with ammonia ligands prefer to occupy Rydberg orbitals rather than antibonding orbitals between Mo and N₂. This result is in line with the recent literature on weakly bound electrons in the periphery of metal complexes, which have been shown to have strong reducing power, ⁶⁴ a topic that will be examined in a future study.

ASSOCIATED CONTENT

Supporting Information

The Supporting Information is available free of charge at https://pubs.acs.org/doi/10.1021/acs.jpca.3c07801.

Details on MRCI and CASSCF calculations, comparison of different density functionals, solvent effects, spin states, extended molecular orbital diagrams, discussion on occupied Rydberg orbitals (PDF)

Ligand field effects on molybdenum for N_2 binding (TXT)

AUTHOR INFORMATION

Corresponding Authors

Evangelos Miliordos — Department of Chemistry and Biochemistry, Auburn University, Auburn, Alabama 36849-5312, United States; orcid.org/0000-0003-3471-7133; Email: ezm0048@auburn.edu

Konstantinos D. Vogiatzis — Department of Chemistry, University of Tennessee, Knoxville, Tennessee 37996-1600, United States; orcid.org/0000-0002-7439-3850; Email: kvogiatz@utk.edu

Authors

Maria V. White – Department of Chemistry, University of Tennessee, Knoxville, Tennessee 37996-1600, United States Emily E. Claveau – Department of Chemistry and Biochemistry, Auburn University, Auburn, Alabama 36849-5312, United States

Complete contact information is available at: https://pubs.acs.org/10.1021/acs.jpca.3c07801

Notes

The authors declare no competing financial interest.

ACKNOWLEDGMENTS

We gratefully acknowledge the National Science Foundation (CHE-1800237) for the financial support of this work and the Advanced Computer Facility (ACF) of the University of Tennessee for computational resources.

REFERENCES

- (1) Erisman, J. W.; Sutton, M. A.; Galloway, J.; Klimont, Z.; Winiwarter, W. How a century of ammonia synthesis changed the world. *Nat. Geosci.* **2008**, *1*, 636–639.
- (2) Sekiguchi, Y.; Arashiba, K.; Tanaka, H.; Eizawa, A.; Nakajima, K.; Yoshizawa, K.; Nishibayashi, Y. Catalytic reduction of molecular dinitrogen to ammonia and hydrazine using vanadium complexes. *Angew. Chem., Int. Ed.* **2018**, *57*, 9064–9068.

- (3) Anderson, J. S.; Rittle, J.; Peters, J. C. Catalytic conversion of nitrogen to ammonia by an iron model complex. *Nature* **2013**, *501*, 84–87.
- (4) Arashiba, K.; Miyake, Y.; Nishibayashi, Y. A molybdenum complex bearing pnp-type pincer ligands leads to the catalytic reduction of dinitrogen into ammonia. *Nat. Chem.* **2011**, *3*, 120–125.
- (5) Fajardo, J.; Peters, J. C. Catalytic nitrogen-to-ammonia conversion by osmium and ruthenium complexes. *J. Am. Chem. Soc.* **2017**, *139*, 16105–16108.
- (6) Doyle, L. R.; Wooles, A. J.; Jenkins, L. C.; Tuna, F.; McInnes, E. J.; Liddle, S. T. Catalytic dinitrogen reduction to ammonia at a triamidoamine—titanium complex. *Angew. Chem., Int. Ed.* **2018**, *57*, 6314—6318.
- (7) Kuriyama, S.; Arashiba, K.; Tanaka, H.; Matsuo, Y.; Nakajima, K.; Yoshizawa, K.; Nishibayashi, Y. Direct transformation of molecular dinitrogen into ammonia catalyzed by cobalt dinitrogen complexes bearing anionic pnp pincer ligands. *Angew. Chem., Int. Ed.* **2016**, *55*, 14291–14295.
- (8) Siedschlag, R. B.; Bernales, V.; Vogiatzis, K. D.; Planas, N.; Clouston, L. J.; Bill, E.; Gagliardi, L.; Lu, C. C. Catalytic silylation of dinitrogen with a dicobalt complex. *J. Am. Chem. Soc.* **2015**, *137*, 4638–4641.
- (9) Ma, X.-L.; Li, M.; Lu, J.-B.; Xu, C.-Q.; Li, J. Recent developments of dinitrogen activation on metal complexes and clusters. *Chin. J. Struct. Chem.* **2022**, *41*, 2212080–2212088.
- (10) Tanabe, Y.; Nishibayashi, Y. Comprehensive insights into synthetic nitrogen fixation assisted by molecular catalysts under ambient or mild conditions. *Chem. Soc. Rev.* **2021**, *50*, 5201–5242.
- (11) Yandulov, D. V.; Schrock, R. R. Catalytic reduction of dinitrogen to ammonia at a single molybdenum center. *Science* **2003**, 301, 76–78.
- (12) Ashida, Y.; Mizushima, T.; Arashiba, K.; Egi, A.; Tanaka, H.; Yoshizawa, K.; Nishibayashi, Y. Catalytic production of ammonia from dinitrogen employing molybdenum complexes bearing n-heterocyclic carbene-based pcp-type pincer ligands. *Nat. Synth.* **2023**, *2*, 635–644.
- (13) Ashida, Y.; Arashiba, K.; Tanaka, H.; Egi, A.; Nakajima, K.; Yoshizawa, K.; Nishibayashi, Y. Molybdenum-catalyzed ammonia formation using simple monodentate and bidentate phosphines as auxiliary ligands. *Inorg. Chem.* **2019**, *58*, 8927–8932.
- (14) Buscagan, T. M.; Rees, D. C. Rethinking the nitrogenase mechanism: Activating the active site. *Joule* **2019**, *3*, 2662–2678.
- (15) Fryzuk, M. D.; Haddad, T.; Mylvaganam, M.; McConville, D. H.; Rettig, S. J. End-on versus side-on bonding of dinitrogen to dinuclear early transition-metal complexes. *J. Am. Chem. Soc.* **1993**, 115, 2782–2792.
- (16) Fryzuk, M. D.; Johnson, S. A. The continuing story of dinitrogen activation. *Coord. Chem. Rev.* **2000**, 200–202, 379–409.
- (17) Fryzuk, M. D.; Johnson, S. A.; Patrick, B. O.; Albinati, A.; Mason, S. A.; Koetzle, T. F. New mode of coordination for the dinitrogen ligand: formation, bonding, and reactivity of a tantalum complex with a bridging n2 unit that is both side-on and end-on. *J. Am. Chem. Soc.* **2001**, *123*, 3960–3973.
- (18) Fryzuk, M. D. Side-on end-on bound dinitrogen: An activated bonding mode that facilitates functionalizing molecular nitrogen. *Acc. Chem. Res.* **2009**, *42*, 127–133.
- (19) MacLachlan, E. A.; Fryzuk, M. D. Synthesis and reactivity of side-on-bound dinitrogen metal complexes. *Organometallics* **2006**, *25*, 1530–1543.
- (20) Burford, R. J.; Fryzuk, M. D. Examining the relationship between coordination mode and reactivity of dinitrogen. *Nat. Rev. Chem* **2017**, *1*, 0026.
- (21) Tanabe, Y.; Nishibayashi, Y. Developing more sustainable processes for ammonia synthesis. *Coord. Chem. Rev.* **2013**, 257, 2551–2564.
- (22) Tanabe, Y.; Nishibayashi, Y. Catalytic Dinitrogen Fixation to Form Ammonia at Ambient Reaction Conditions Using Transition Metal-Dinitrogen Complexes. *Chem. Rec.* **2016**, *16*, 1549–1577.

- (23) Bezdek, M. J.; Chirik, P. J. Expanding boundaries: N2 cleavage and functionalization beyond early transition metals. *Angew. Chem., Int. Ed.* **2016**, *55*, 7892–7896.
- (24) MacLeod, K. C.; Vinyard, D. J.; Holland, P. L. A multi-iron system capable of rapid n2 formation and n2 cleavage. *J. Am. Chem. Soc.* **2014**, 136, 10226–10229.
- (25) Zhang, G.; Liu, T.; Song, J.; Quan, Y.; Jin, L.; Si, M.; Liao, Q. N2 cleavage on d4/d4 molybdenum centers and its further conversion into iminophosphorane under mild conditions. *J. Am. Chem. Soc.* **2022**, *144*, 2444–2449.
- (26) Taylor, L. J.; Kays, D. L. Low-coordinate first-row transition metal complexes in catalysis and small molecule activation. *Dalton Trans.* **2019**, *48*, 12365–12381.
- (27) Pierpont, A. W.; Cundari, T. R. Dinitrogen activation by low-coordinate transition metal complexes. *J. Coord. Chem.* **2011**, *64*, 3123–3135.
- (28) Yamout, L. S.; Ataya, M.; Hasanayn, F.; Holland, P. L.; Miller, A. J.; Goldman, A. S. Understanding terminal versus bridging end-on n2 coordination in transition metal complexes. *J. Am. Chem. Soc.* **2021**, *143*, 9744–9757.
- (29) Hasanayn, F.; Holland, P. L.; Goldman, A. S.; Miller, A. J. Lewis structures and the bonding classification of end-on bridging dinitrogen transition metal complexes. *J. Am. Chem. Soc.* **2023**, *145*, 4326–4342.
- (30) Egi, A.; Tanaka, H.; Yoshizawa, K. Theoretical views on catalytic reaction pathways for nitrogen fixation by dinitrogen-bridging dimolybdenum complexes. *J. Synth. Org. Chem., Jpn.* **2021**, 79, 1041–1049.
- (31) Sader, S.; Miliordos, E. Methane to methanol conversion facilitated by anionic transition metal centers: The case of fe, ni, pd, and pt. *J. Phys. Chem. A* **2021**, *125*, 2364–2373.
- (32) Sader, S.; Miliordos, E. Being negative can be positive: metal oxide anions promise more selective methane to methanol conversion. *Phys. Chem. Chem. Phys.* **2022**, *24*, 21583–21587.
- (33) White, M. V.; Kirkland, J. K.; Vogiatzis, K. D. Redox states of dinitrogen coordinated to a molybdenum atom. *J. Chem. Phys.* **2021**, 154, 224308.
- (34) Vogiatzis, K. D.; Polynski, M. V.; Kirkland, J. K.; Townsend, J.; Hashemi, A.; Liu, C.; Pidko, E. A. Computational approach to molecular catalysis by 3d transition metals: Challenges and opportunities. *Chem. Rev.* **2019**, *119*, 2453–2523.
- (35) Roos, B. O.; Taylor, P. R.; Sigbahn, P. E. A complete active space scf method (casscf) using a density matrix formulated super-ci approach. *Chem. Phys.* **1980**, *48*, 157–173.
- (36) Olsen, J.; Roos, B. O.; Jo/rgensen, P.; Jensen, H. J. A. Determinant based configuration interaction algorithms for complete and restricted configuration interaction spaces. *J. Chem. Phys.* **1988**, 89, 2185–2192.
- (37) Knowles, P. J.; Werner, H.-J. An efficient method for the evaluation of coupling coefficients in configuration interaction calculations. *Chem. Phys. Lett.* **1988**, *145*, 514–522.
- (38) Werner, H.-J.; Knowles, P. J. An efficient internally contracted multiconfiguration—reference configuration interaction method. *J. Chem. Phys.* **1988**, *89*, 5803—5814.
- (39) Dunning, T. H. Gaussian basis sets for use in correlated molecular calculations. i. the atoms boron through neon and hydrogen. *J. Chem. Phys.* **1989**, *90*, 1007–1023.
- (40) Kendall, R. A.; Dunning, T. H.; Harrison, R. J. Electron affinities of the first-row atoms revisited. systematic basis sets and wave functions. *J. Chem. Phys.* **1992**, *96*, 6796–6806.
- (41) Peterson, K. A.; Figgen, D.; Dolg, M.; Stoll, H. Energy-consistent relativistic pseudopotentials and correlation consistent basis sets for the 4d elements y-pd. *J. Chem. Phys.* **2007**, *126*, 124101.
- (42) Werner, H.-J.; Knowles, P. J.; Knizia, G.; Manby, F. R.; Schütz, M. Molpro: a general-purpose quantum chemistry program package. *Wiley Interdiscip. Rev.: Comput. Mol. Sci.* **2012**, *2*, 242–253.
- (43) Frisch, M. J.; Trucks, G. W.; Schlegel, H. B.; Scuseria, G. E.; Robb, M. A.; Cheeseman, J. R.; Scalmani, G.; Barone, V.; Petersson, G. A.; Nakatsuji, H.; Li, X.; Caricato, M.; Marenich, A. V.; Bloino, J.;

- Janesko, B. G.; Gomperts, R.; Mennucci, B.; Hratchian, H. P.; Ortiz, J. V.; Izmaylov, A. F.; Sonnenberg, J. L.; Williams-Young, D.; Ding, F.; Lipparini, F.; Egidi, F.; Goings, J.; Peng, B.; Petrone, A.; Henderson, T.; Ranasinghe, D.; Zakrzewski, V. G.; Gao, J.; Rega, N.; Zheng, G.; Liang, W.; Hada, M.; Ehara, M.; Toyota, K.; Fukuda, R.; Hasegawa, J.; Ishida, M.; Nakajima, T.; Honda, Y.; Kitao, O.; Nakai, H.; Vreven, T.; Throssell, K.; Montgomery, J. A., Jr.; Peralta, J. E.; Ogliaro, F.; Bearpark, M. J.; Heyd, J. J.; Brothers, E. N.; Kudin, K. N.; Staroverov, V. N.; Keith, T. A.; Kobayashi, R.; Normand, J.; Raghavachari, K.; Rendell, A. P.; Burant, J. C.; Iyengar, S. S.; Tomasi, J.; Cossi, M.; Millam, J. M.; Klene, M.; Adamo, C.; Cammi, R.; Ochterski, J. W.; Martin, R. L.; Morokuma, K.; Farkas, O.; Foresman, J. B.; Fox, D. J. Gaussian 16. Revision C.01; Gaussian Inc.: Wallingford CT, 2016.
- (44) Kirkland, J. K.; Khan, S. N.; Casale, B.; Miliordos, E.; Vogiatzis, K. D. Ligand field effects on the ground and excited states of reactive feo 2+ species. *Phys. Chem. Chem. Phys.* **2018**, *20*, 28786–28795.
- (45) Neese, F. Software update: The orca program system—version 5.0. Wiley Interdiscip. Rev.: Comput. Mol. Sci. 2022, 12, No. e1606.
- (46) Weigend, F.; Ahlrichs, R. Balanced basis sets of split valence, triple zeta valence and quadruple zeta valence quality for h to rn: Design and assessment of accuracy. *Phys. Chem. Chem. Phys.* **2005**, 7, 3297–3305.
- (47) Weigend, F. Accurate coulomb-fitting basis sets for h to rn. *Phys. Chem. Phys.* **2006**, 8, 1057–1065.
- (48) Lee, C.; Yang, W.; Parr, R. G. Development of the colle-salvetti correlation-energy formula into a functional of the electron density. *Phys. Rev. B* **1988**, *37*, 785–789.
- (49) Becke, A. D. Density-functional thermochemistry. III. The role of exact exchange. *J. Chem. Phys.* **1993**, *98*, 5648–5652.
- (50) Caldeweyher, E.; Bannwarth, C.; Grimme, S. Extension of the d3 dispersion coefficient model. *J. Chem. Phys.* **2017**, *147*, 034112.
- (51) Caldeweyher, E.; Ehlert, S.; Hansen, A.; Neugebauer, H.; Spicher, S.; Bannwarth, C.; Grimme, S. A generally applicable atomic-charge dependent london dispersion correction. *J. Chem. Phys.* **2019**, *150*, 154122.
- (52) Barone, V.; Cossi, M. Quantum calculation of molecular energies and energy gradients in solution by a conductor solvent model. *J. Phys. Chem. A* **1998**, *102*, 1995–2001.
- (53) Zhao, J.; Chen, Z. Single mo atom supported on defective boron nitride monolayer as an efficient electrocatalyst for nitrogen fixation: A computational study. *J. Am. Chem. Soc.* **2017**, *139*, 12480–12487.
- (54) Geng, J.; Zhang, S.; Xu, H.; Wang, G.; Zhang, H. An oxygen-coordinated molybdenum single atom catalyst for efficient electrosynthesis of ammonia. *Chem. Commun.* **2021**, *57*, 5410–5413.
- (55) Kuhlman, M. L.; Flowers, R. A., II Aggregation state and reducing power of the samarium diiodide—dmpu complex in acetonitrile. *Tetrahedron Lett.* **2000**, *41*, 8049–8052.
- (56) Basolo, F.; Pearson, R. G. The trans effect in metal complexes. *Progress in inorganic chemistry*; Wiley, 2009; Vol. 4, pp 381–453.
- (57) Takasu, R.; Misaizu, F.; Hashimoto, K.; Fuke, K. Microscopic solvation process of alkali atoms in finite clusters: Photoelectron and photoionization studies of $M(NH_3)^n$ and $M(H_2O)_n$ (M = Li, Li⁻, Na⁻). *J. Phys. Chem. A* **1997**, *101*, 3078–3087.
- (58) Jackson, B. A.; Khan, S. N.; Miliordos, E. A fresh perspective on metal ammonia molecular complexes and expanded metals: opportunities in catalysis and quantum information. *Chem. Commun.* **2023**, *59*, 10572–10587.
- (59) Hartweg, S.; Barnes, J.; Yoder, B. L.; Garcia, G. A.; Nahon, L.; Miliordos, E.; Signorell, R. Solvated dielectrons from optical excitation: An effective source of low-energy electrons. *Science* **2023**, 380, 1161–1165.
- (60) Almeida, N. M. S.; Pawłowski, F.; Ortiz, J. V.; Miliordos, E. Transition-metal solvated-electron precursors: diffuse and 3d electrons in $V(NH_3)0,\pm 6$. Phys. Chem. Chem. Phys. **2019**, 21, 7090–7097.
- (61) Jackson, B. A.; Miliordos, E. Electronic and geometric structure of cationic and neutral chromium and molybdenum ammonia complexes. *J. Chem. Phys.* **2021**, *155*, 014303.

- (62) Ariyarathna, I. R.; Miliordos, E. Dative bonds versus electron solvation in tri-coordinated beryllium complexes: Be(cx)3 [x = 0, s, se, te, po] and be(ph3)3 versus be(nh3)3. *Int. J. Quantum Chem.* **2018**, 118, No. e25673.
- (63) Fries, D. V.; Klein, M. P.; Straßner, A.; Huber, M. E.; Niedner-Schatteburg, G. Cryo-IR spectroscopy and cryo-kinetics of cluster N2 adsorbate complexes of tantalum cluster cations Ta5-8+. *J. Chem. Phys.* **2023**, *159* (16), *164306*.
- (64) Jackson, B. A.; Miliordos, E. Simultaneous co₂ capture and functionalization: solvated electron precursors as novel catalysts. *Chem. Commun.* **2022**, *58*, 1310–1313.